Applied Radiation and Isotopes 200 (2023) 110954

Contents lists available at ScienceDirect

Applied Radiation and Isotopes

journal homepage: www.elsevier.com/locate/apradiso

Cross-section measurement of thulium radioisotopes with an 18 MeV medical PET cyclotron for an optimized ^{165}Er production

Gaia Dellepiane [a,*], Pierluigi Casolaro [a], Chiara Favaretto [b,c], Alexander Gottstein [a], Pascal V. Grundler [b], Isidre Mateu [a], Edoardo Renaldin [b], Paola Scampoli [a,d], Zeynep Talip [b], Nicholas P. van der Meulen [b,e], Saverio Braccini [a]

[a] Albert Einstein Center for Fundamental Physics (AEC), Laboratory for High Energy Physics (LHEP), University of Bern, Sidlerstrasse 5, CH-3012 Bern, Switzerland
[b] Center for Radiopharmaceutical Sciences, ETH-PSI-USZ, Paul Scherrer Institute, 5232 Villigen-PSI, Switzerland
[c] Division of Nuclear Medicine, University Hospital Basel, 4031 Basel, Switzerland
[d] Department of Physics "Ettore Pancini", University of Napoli Federico II, Complesso Universitario di Monte S. Angelo, 80126 Napoli, Italy
[e] Laboratory of Radiochemistry, Paul Scherrer Institute, 5232 Villigen-PSI, Switzerland

ARTICLE INFO

Keywords:
Erbium-165
Auger electrons
Targeted radionuclide therapy
Cross sections
Proton irradiation
Medical cyclotron
Solid targets

ABSTRACT

^{165}Er is a pure Auger-electron emitter with promising characteristics for therapeutic applications in nuclear medicine. The short penetration path and high Linear Energy Transfer (LET) of the emitted Auger electrons make ^{165}Er particularly suitable for treating small tumor metastases. Several production methods based on the irradiation with charged particles of Er and Ho targets can be found in the literature. In this paper, we report on the study of ^{165}Er indirect production performed via the ^{166}Er(p,2n)^{165}Tm → ^{165}Er reaction at the 18 MeV Bern medical cyclotron. Despite the use of highly enriched $^{166}Er_2O_3$ targets, several Tm radioisotopes are produced during the irradiation, making the knowledge of the cross sections involved crucial. For this reason, a precise investigation of the cross sections of the relevant nuclear reactions in the energy range of interest was performed by irradiating Er_2O_3 targets with different isotopic enrichment levels and using a method based on the inversion of a linear system of equations. For the reactions ^{164}Er(p, γ)^{165}Tm, ^{166}Er(p,n)^{166}Tm, ^{166}Er(p, γ)^{167}Tm, ^{167}Er(p,3n)^{165}Tm, ^{167}Er(p, γ)^{168}Tm, ^{168}Er(p,2n)^{167}Tm and ^{170}Er(p,3n)^{168}Tm, the nuclear cross section was measured for the first time. From the results obtained, the production yield and purity of the parent radioisotope ^{165}Tm were calculated to assess the optimal irradiation conditions. Several production tests with solid targets were performed to confirm these findings.

1. Introduction

Targeted radionuclide therapy is a promising strategy for cancer treatment. It is based on the use of radiopharmaceuticals that selectively target diseased cells, limiting the exposure of surrounding healthy tissue. This makes it possible to also treat metastatic or disseminated tumors, for which surgery and radiotherapy are not feasible. The radionuclide used to label the vector molecule is an α-, β^-- or Auger-electron emitter, which is responsible for the efficacy of the treatment.

Auger-electron-emitting radionuclides are receiving increasing interest as therapeutic agents thanks to their potentially high level of cytotoxicity (Kassis and Adelstein, 2005). This is due to their high LET (between 4 and 25 keV/μm) resulting in cell damage, both from indirect interaction through radical formation and direct-double-strand breaks (Ku et al., 2019). Furthermore, their range in tissue, of the order of 1 μm, reduces their toxicity beyond the targeted cell (Falzone et al., 2012). These characteristics make them particularly suitable for the treatment of small metastatic tumor lesions.

Among Auger-emitting radionuclides, ^{165}Er [$t_{1/2}$ = 10.36 h, ec: 100%] shows promising characteristics due to its decay through electron capture, resulting in the emission of 5.3 keV (65.6%) and 38.4 keV (4.8%) Auger electrons and low-energy X-rays [E_X = 47.6 keV (38.1%); 46.7 keV (21.4%)]. The absence of gamma emissions avoids additional dose absorption by the patient and makes it interesting as a pure Auger-electron emitter for in-depth investigations on the biological effect of Auger electrons alone. The Auger-electron energies emitted by ^{165}Er are similar to those of the intensely-studied ^{125}I [$t_{1/2}$ = 59.4 d, ec: 100%] (Yasui et al., 2001; Kassis, 2004), however, the similar chemical

* Corresponding author.
E-mail address: gaia.dellepiane@lhep.unibe.ch (G. Dellepiane).

https://doi.org/10.1016/j.apradiso.2023.110954
Received 26 May 2023; Received in revised form 18 July 2023; Accepted 19 July 2023
Available online 24 July 2023

Table 1
^{165}Er production routes.

Impinging particle	Target	Route
p	^{165}Ho	^{165}Ho(p,n)^{165}Er (Beyer et al., 2004; Tárkányi et al., 2008b; Zandi et al., 2013; Gracheva et al., 2020)
	^{nat}Er	^{nat}Er(p,x)^{165}Tm →^{165}Er (Tárkányi et al., 2008c, 2009; Zandi et al., 2013)
	^{166}Er	^{166}Er(p,2n)^{165}Tm →^{165}Er (Sadeghi et al., 2010; Zandi et al., 2013)
d	^{165}Ho	^{165}Ho(d,2n)^{165}Er (Tárkányi et al., 2008a; Zandi et al., 2013; Hermanne et al., 2013)
	^{nat}Er	^{nat}Er(d,x)^{165}Tm →^{165}Er (Tárkányi et al., 2007)
	^{164}Er	^{164}Er(d,n)^{165}Tm →^{165}Er (Sadeghi et al., 2010)
	^{166}Er	^{166}Er(d,3n)^{165}Tm →^{165}Er (Sadeghi et al., 2010)

characteristics of lanthanides (Cotton, 2006; Sadler et al., 2022) allows ^{165}Er to be labeled in a similar manner as is practised with ^{177}Lu. ^{165}Er can be produced via several charged-particle-induced reactions, as reported in Table 1.

Direct production via the ^{165}Ho(p,n)^{165}Er reaction allows the use of monoisotopic holmium, which is reasonably priced. In a previous publication, we reported on the production of 1.6 GBq of ^{165}Er, obtained by irradiating a 10-mm-diameter ^{nat}Ho target with about 10 μA protons for 10 h (Gracheva et al., 2020). A separation procedure of about 10 h resulted in a radionuclidic purity above 99.9%. However, considering the ^{165}Er half-life of 10.4 h, this resulted in a considerable loss of activity. Moreover, further analysis revealed the presence of large amounts of non-radioactive Er in the product, due to Er occurring naturally in Ho material, thereby preventing effective radiolabeling. Large-scale production could be performed if one used large targets, however, the chemistry would have to be adjusted as a result. This would likely still compromise the product yield.

In the framework of a research program focused on novel radionuclides for theranostics at the Bern medical cyclotron laboratory, the indirect production of ^{165}Er via the reaction ^{166}Er(p,2n)^{165}Tm → ^{165}Er was investigated by irradiating natural Er_2O_3 and enriched $^{166}Er_2O_3$ targets. The isotopic compositions of the materials are reported in Table 2.

In both cases, many thulium radioisotopes are produced during the irradiation (Table 3). The main impurities to be kept under control in the energy range of PET medical cyclotrons are ^{166}Tm, obtained from ^{166}Er and ^{167}Er via the ^{166}Er(p,n)^{166}Tm and ^{167}Er(p,2n)^{166}Tm nuclear reactions, respectively, and ^{167}Tm, obtained from ^{166}Er, ^{167}Er and ^{168}Er via the ^{166}Er(p, γ)^{167}Tm, ^{167}Er(p,n)^{167}Tm and ^{168}Er(p,2n)^{167}Tm nuclear reactions, respectively.

Because Tm impurities decay into stable isotopes of Er, it is necessary to minimize their production to optimize the purity of the eluted ^{165}Er. The precise knowledge of the cross sections as a function of the beam energy is therefore of paramount importance.

In this paper, we report on the cross-section measurements performed with the Beam Transport Line (BTL) at the Bern medical cyclotron. The contribution to the cross section of each nuclear reaction was determined using a method based on the inversion of a linear system of equations.

The results were used to assess the irradiation conditions that optimize the ^{165}Tm production. On this basis, production irradiation tests from enriched $^{166}Er_2O_3$ solid targets were performed.

2. Material and methods

The Bern medical cyclotron laboratory at the Bern University Hospital (Inselspital) (Braccini, 2013) features an IBA Cyclone 18/18 HC (nominal energy 18 MeV, current range from a few pA to 150 μA Auger

Table 2
Isotopic fractions in natural Er_2O_3 (Meija et al., 2016), enriched $^{166}Er_2O_3$ and enriched $^{167}Er_2O_3$ powder obtained from ISOFLEX (California, USA) (Isoflex, 2022).

	^{162}Er	^{164}Er	^{166}Er	^{167}Er	^{168}Er	^{170}Er
Natural Er_2O_3 [%]	0.139	1.601	33.503	22.869	26.978	14.910
Enr.$^{166}Er_2O_3$ [%]	0.01	0.02	98.1	1.33	0.45	0.10
Enr.$^{167}Er_2O_3$ [%]	0	0.01	0.96	96.30	2.57	0.16
Enr.$^{168}Er_2O_3$ [%]	0	0	0.37	0.72	98.30	0.61

Table 3
Decay properties of thulium radioisotopes (Abriola and Verpelli, 2011; Jain et al., 2006; Baglin, 2008, 2000, 2010; Baglin et al., 2018). The values in parentheses are the uncertainties referred to the last digits of the value.

Radioisotope	$t_{1/2}$	Decay mode: [%]	E_γ [keV]	BR [%]
^{165}Tm	30.06*(3)* h	ec + β^+: 100	242.917*(7)*	35.5*(17)*
^{166}Tm	7.70*(3)* h	ec + β^+: 100	778.814*(15)*	19.1*(12)*
^{167}Tm	9.25*(2)* d	ec: 100	207.801*(15)*	42*(8)*
^{168}Tm	93.1*(2)* d	ec + β^+: 99.990	198.251*(2)*	54.49*(16)*
^{170}Tm	128.6*(3)* d	β^-: 99.869	84.25474*(8)*	2.48*(6)*

et al., 2015) equipped with six ^{18}O-enriched water targets, an IBA Nirta solid target station and a 6-m-long BTL. The BTL brings the beam to a second bunker with independent access, allowing the spin-off company Swan Isotopen AG to synthesize ^{18}F-labeled tracers for PET imaging overnight and the Laboratory for High Energy Physics (LHEP) of the University of Bern to perform multidisciplinary research during the day (Braccini and Scampoli, 2016).

The BTL is equipped with beam focusing and diagnostic systems, including a non-destructive two-dimensional beam profiler based on scintillating doped silica fibers passing through the beam. The detector, named UniBEaM, was developed by LHEP and is commercialized by the company D-Pace (Auger et al., 2016; Potkins et al., 2017). The BTL is characterized by an extracted beam energy of (18.3 ± 0.4) MeV (Nesteruk et al., 2018; Häffner et al., 2019) and was used for the cross-section measurements presented in this paper.

2.1. Materials and procedures for cross-section measurements

Targets for cross-section measurements were prepared using the sedimentation method on aluminum discs (Fig. 1-a: 22.8 mm in diameter, 2 mm thick). A few milligrams of Er_2O_3 were suspended in absolute ethanol (EtOH) and deposited in the 4.2-mm-diameter, 0.8-mm-deep pocket in the middle of the disc (Fig. 1-b). Once the ethanol had completely evaporated, the mass deposited was assessed using an analytical balance (Mettler Toledo XS204 DeltaRange) and covered with a 13-μm-thin aluminum foil (Fig. 1-c) to ensure that no leakage would occur during the irradiation and measurement procedures.

With this method, it was possible to produce targets with an average thickness of about 25 μm, allowing the beam energy to be considered constant within the uncertainty over the full irradiated mass.

Each target was irradiated with a proton beam with a flat surface distribution, so that any inhomogeneities in thickness due to sedimentation could be neglected. This procedure, successfully used in our previous works on cross-section measurements (Dellepiane et al., 2022a,d,b, 2023), is described in detail in Carzaniga et al. (2017).

The beam was flattened by the optical elements of the BTL and monitored online with the UniBEaM detector. A custom target station, providing a controlled-diameter beam thanks to an 8-mm collimator, was connected to an electrometer (B2985 A Keysight) to measure the beam current hitting the target. To perform irradiations below 18 MeV, the beam energy was degraded by means of aluminum attenuator discs placed in front of the target and was determined using the SRIM-2013 Monte Carlo code (Ziegler and Manoyan, 1988).

The activities at End of Bombardment (EoB) were assessed by gamma spectrometry using a N-type High Purity Germanium (HPGe) detector (Canberra2019). The detector was coupled to a preamplifier

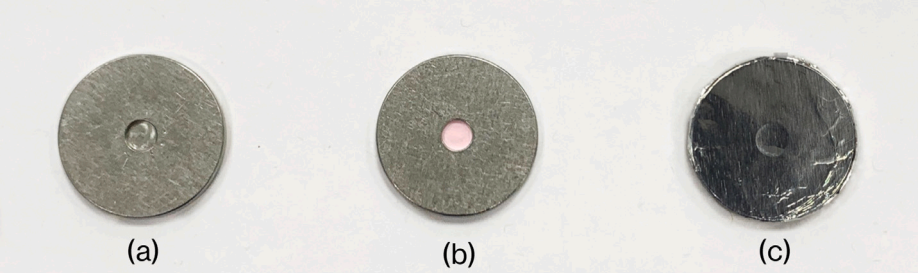

Fig. 1. Preparation procedure for the targets used for cross-section measurements: (a) empty aluminum disc; (b) aluminum disc filled with erbium oxide; (c) aluminum disc covered with a 13-μm-thick aluminum foil.

and to a Lynx® digital signal analyzer. The spectrum of the source was acquired with the Genie2K software (Mirion Technologies, 2022) in the case of a single measurement and with the Excel2Genie (Forgács et al., 2014) Microsoft Excel application for repeated measurements. The analysis was performed with the InterSpec software (Sandia National Laboratories, 2022), developed by Sandia National Laboratories. The efficiency calibration was performed in accordance with the international standard (International Standard, 2021) by means of a multi-peak γ-source, and resulted in efficiency uncertainties below 3% (Durán et al., 2022; Juget et al., 2023).

For Tm radioisotopes whose production is the result of two or more nuclear processes, it was necessary to decouple their contributions to the production cross section. For this purpose, a method based on the inversion of a linear system of equations was used (Braccini et al., 2022; Dellepiane et al., 2022c). This method requires measuring the total cross section with as many materials, with different isotopic compositions, as the number of the reactions involved in the production of the radionuclide being considered.

For radionuclides produced by three reactions, a third enriched material had to be included. For this purpose, the cross sections measured from enriched $^{167}Er_2O_3$ and enriched $^{168}Er_2O_3$ powder (Table 2) as a part of a research program on the production of ^{167}Tm for medical applications were considered. The results of this study will be published in a forthcoming paper (Renaldin et al., 2023).

As an example, in the energy range of interest, ^{167}Tm is produced by three nuclear reactions, namely ^{166}Er(p, γ)^{167}Tm, ^{167}Er(p,n)^{167}Tm and ^{168}Er(p,2n)^{167}Tm.

For a given beam energy, the following linear system holds:

$$\begin{pmatrix} \sigma_i(^{167}Tm) \\ \sigma_j(^{167}Tm) \\ \sigma_k(^{167}Tm) \end{pmatrix} = \begin{pmatrix} \epsilon_{i,166} & \epsilon_{i,167} & \epsilon_{i,168} \\ \epsilon_{j,166} & \epsilon_{j,167} & \epsilon_{j,168} \\ \epsilon_{k,166} & \epsilon_{k,167} & \epsilon_{k,168} \end{pmatrix} \cdot \begin{pmatrix} \sigma(^{166}Er(p,\gamma)^{167}Tm) \\ \sigma(^{167}Er(p,n)^{167}Tm) \\ \sigma(^{168}Er(p,2n)^{167}Tm) \end{pmatrix} \quad (1)$$

where on the left there are the experimentally-measured production cross sections with the three materials enriched in i,j,k=^{166}Er, ^{167}Er, ^{168}Er and, on the right, the nuclear cross sections to be determined. $\epsilon_{i,j,k,16x}$ are the isotopic abundances of the Er isotopes in the enriched materials.

An analogous system of equations holds for the other Tm radioisotopes.

The targets were irradiated for an average of 8 min with a mean current of 6 nA and measured with the HPGe detector at staged times, in order to exploit the difference in the half-lives of the thulium radioisotopes. In all measurements, the dead time was below 1%. The γ-lines used to identify the radionuclides of interest are listed in Table 3.

2.2. Material and procedures for ^{165}Er production tests

Two targets were prepared for the production tests by compressing approximately 68 and 35 mg of enriched $^{166}Er_2O_3$ powder, in order to verify the impact of the target thickness on radionuclidic purity. The mass and thickness of the disc-shaped pellets (6 mm in diameter) were accurately measured to determine the experimental density, resulting in (5.08 ± 0.01) g/cm^3. This value was used in all calculations and SRIM simulations.

For the irradiation, the pellets were placed in a special capsule – called coin – consisting of two aluminum halves held together by small magnets.

The thickness of the front end was used to adjust the energy of the protons reaching the target, in order to optimize the production yield and radionuclidic purity. The back end contained the pellet and an O-ring in order to prevent the possible leakage of solid material or of any gas produced during the irradiation.

The coin was conceived and built by LHEP to irradiate compressed powder pellets or solid foils and has been successfully used to produce several radionuclides (Dellepiane et al., 2021), in particular ^{44}Sc (van der Meulen et al., 2020), ^{68}Ga (Braccini et al., 2022) and ^{155}Tb (Dellepiane et al., 2022a; Favaretto et al., 2021).

The coin containing the enriched $^{166}Er_2O_3$ pellet was placed in an adapted target holder and positioned in the station used for cross-section measurements. In this configuration, high beam intensities cannot be achieved as the station is not equipped with a cooling system.

3. Data analysis and results

3.1. Cross-section measurements

The systematic uncertainty in cross-section measurements was obtained by summing all the contributes in quadrature, estimated to be about 8% including the uncertainty on the flatness of the beam (5%), the beam current integration (1%), the HPGe detector efficiency (3%) and the target mass measurements (5%).

In the case of ^{167}Tm, the main experimental uncertainty was due to the branching ratio of the γ-line, namely ~19%. For ^{170}Tm, the main contribution was the statistical error in the γ-ray counting (~30%), due to the low activities produced. The total uncertainties of the measured cross sections (Tables 5–11) were obtained by summing the systematic and experimental contributions in quadrature.

Thulium-165. In the energy region investigated, ^{165}Tm is produced from ^{164}Er, ^{166}Er and ^{167}Er via the reactions (p, γ), (p,2n) and (p,3n), respectively. The production cross sections measured from natural Er_2O_3 and enriched $^{166}Er_2O_3$ are reported in Fig. 2 together with TENDL-2021 predictions (Koning and Rochman, 2012), which reproduce them reasonably well. In the case of natural Er_2O_3, our results were compared with data available in the literature (Tárkányi et al., 2009), finding a good agreement for energies above 11 MeV. At low energies, some discrepancies were observed.

The nuclear cross sections were calculated using the method described in Section 2.1. For this purpose, the production cross section measured from the enriched $^{167}Er_2O_3$ material and reported in a forthcoming paper (Renaldin et al., 2023) were included. The nuclear cross sections are shown in Fig. 3 together with TENDL-2021 predictions (Koning and Rochman, 2012), which are in good agreement with

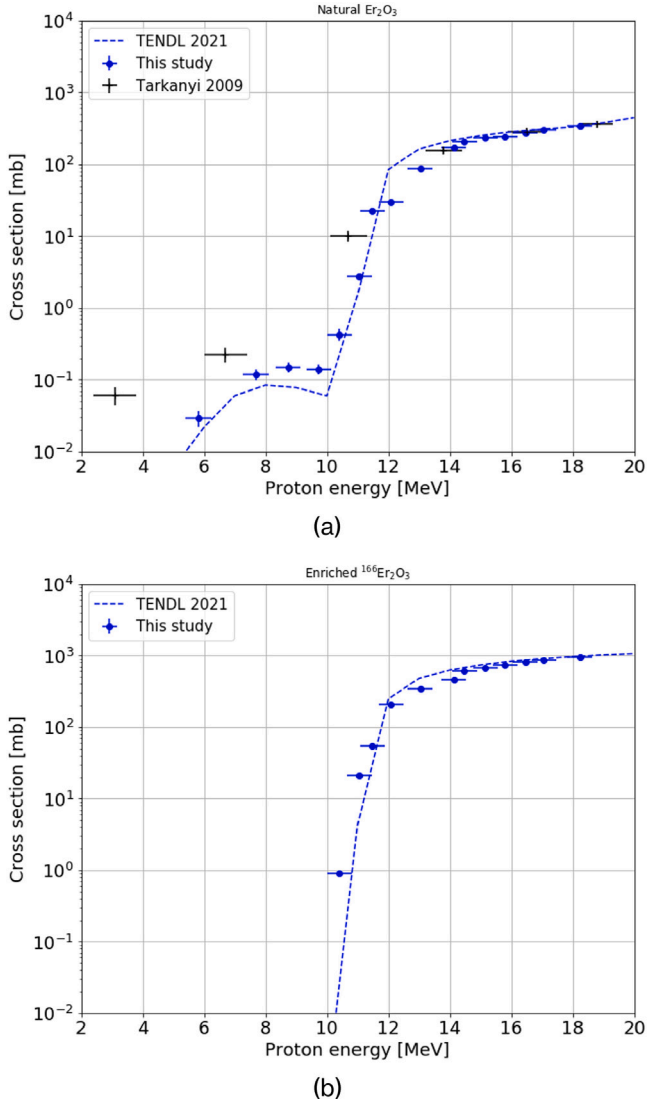

Fig. 2. ^{165}Tm production cross section from natural Er_2O_3 (a) and enriched $^{166}Er_2O_3$ (b) targets, whose isotopic composition is reported in Table 2.

the experimental data. Our findings for the reaction ^{166}Er(p,2n)^{165}Tm are generally compatible with the results reported by Tárkányi et al. (2010).

It was only possible to derive the cross sections of the ^{164}Er(p, γ)^{165}Tm reaction at energies below 11 MeV, corresponding to the threshold energy of the ^{166}Er(p,2n)^{165}Tm reaction. Above this value, the contribution of the latter reaction is strongly predominant. To the best of our knowledge, no cross-section data were reported in the literature for the ^{164}Er(p, γ)^{165}Tm reaction prior to our study. For completeness, the numerical values are reported in the Appendix (Tables 5, 6 and 7).

Thulium-166. Two nuclear reactions produce ^{166}Tm in the energy range of interest, namely, ^{166}Er(p,n) and ^{167}Er(p,2n). The production cross sections measured from natural Er_2O_3 and enriched $^{166}Er_2O_3$ are reported in Fig. 4 together with TENDL-2021 predictions (Koning and Rochman, 2012). In the case of natural Er_2O_3, our results were compared with data available in the literature (Tárkányi et al., 2008c), finding a good agreement.

The nuclear cross sections are shown in Fig. 5 and, for completeness, the numerical values are reported in the Appendix (Tables 5, 6 and 8). A good agreement was observed with both the TENDL-2021 predictions

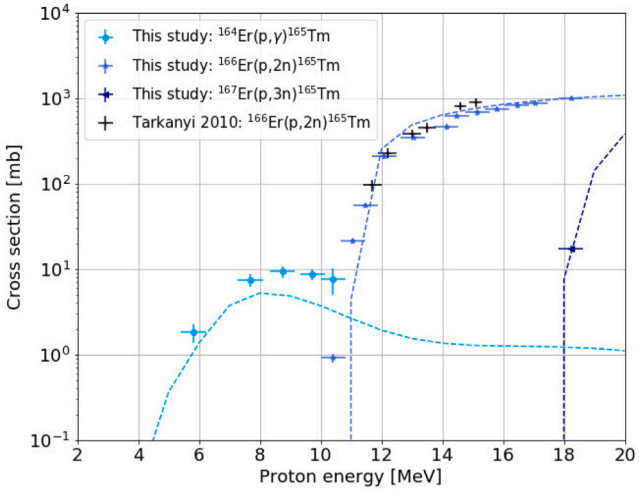

Fig. 3. ^{164}Er(p, γ)^{165}Tm, ^{166}Er(p,2n)^{165}Tm and ^{167}Er(p,3n)^{165}Tm nuclear cross sections. The dots are the experimental data, the dashed lines are the TENDL calculations.

and the experimental data reported in the literature for the reaction ^{167}Er(p,2n)^{166}Tm (Tárkányi et al., 2010). It is worth mentioning that the results reported by Tárkányi et al. (2010) were obtained by subtracting the theoretical contribution of the ^{166}Er(p,n) process, derived from the EMPIRE code (Herman et al., 2007).

The authors are unaware of any data published for the ^{166}Er(p,n)^{166}Tm reaction.

Thulium-167. In the energy range investigated, ^{167}Tm is obtained from the ^{166}Er(p, γ), ^{167}Er(p,n) and ^{168}Er(p,2n) nuclear reactions, respectively. The production cross sections measured from natural Er_2O_3 and enriched $^{166}Er_2O_3$ are reported in Fig. 6 together with TENDL-2021 predictions (Koning and Rochman, 2012), which reproduce them reasonably well. In the case of natural Er_2O_3, our findings were compared with the experimental data available in the literature (Tárkányi et al., 2008c; Hermanne et al., 2011). Some discrepancies with respect to the results published by Tárkányi et al. (2008c) were observed at low energies.

To derive the cross sections for isotopically pure Tm targets, the production cross section measured from enriched $^{167}Er_2O_3$, to be reported in a forthcoming paper (Renaldin et al., 2023), was included. The results are shown in Fig. 7. Experimental data are reported in the literature for the reaction ^{167}Er(p,n)^{167}Tm (Tárkányi et al., 2010), finding a good agreement, while the other reactions are measured in this study for the first time. The results reported by Tárkányi et al. (2010) were obtained by subtracting the theoretical contribution of the ^{168}Er(p,2n) process, derived from the EMPIRE code (Herman et al., 2007), while the ^{166}Er(p, γ) reaction was considered negligible.

The numerical data are reported in the Appendix (Table 5, 6 and 9) for completeness.

Thulium-168. In the energy range of interest, ^{168}Tm is produced from ^{167}Er, ^{168}Er and ^{170}Er via the (p, γ), (p,n) and (p,3n) nuclear reactions, respectively.

It was only possible to measure the production cross section in the case of natural material due to the low isotopic percentage of the target isotopes in the enriched $^{166}Er_2O_3$. The results are reported in Fig. 8, together with TENDL-2021 predictions (Koning and Rochman, 2012) and the experimental data available in the literature (Tárkányi et al., 2008c; Hermanne et al., 2011). A reasonable agreement was found.

The nuclear cross sections were calculated including the measurements performed from enriched $^{167}Er_2O_3$ and enriched $^{168}Er_2O_3$, to be reported in a forthcoming paper (Renaldin et al., 2023). In Fig. 9, the results are compared with the findings reported by Tárkányi et al.

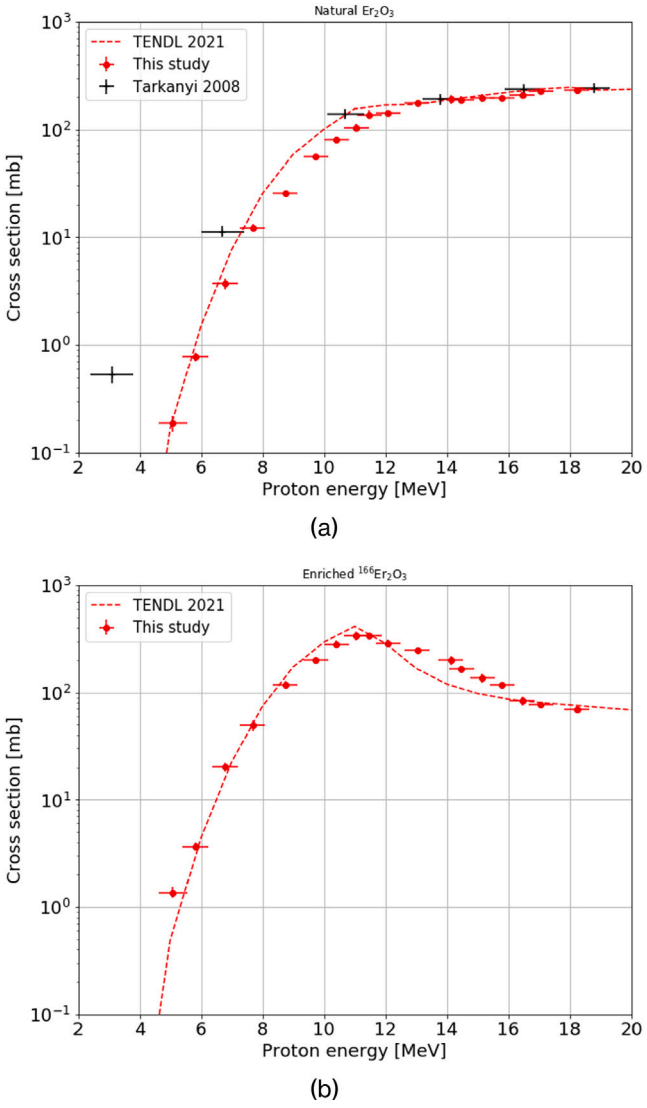

Fig. 4. ^{166}Tm production cross section from natural Er_2O_3 (a) and enriched $^{166}Er_2O_3$ (b) targets, whose isotopic composition is reported in Table 2.

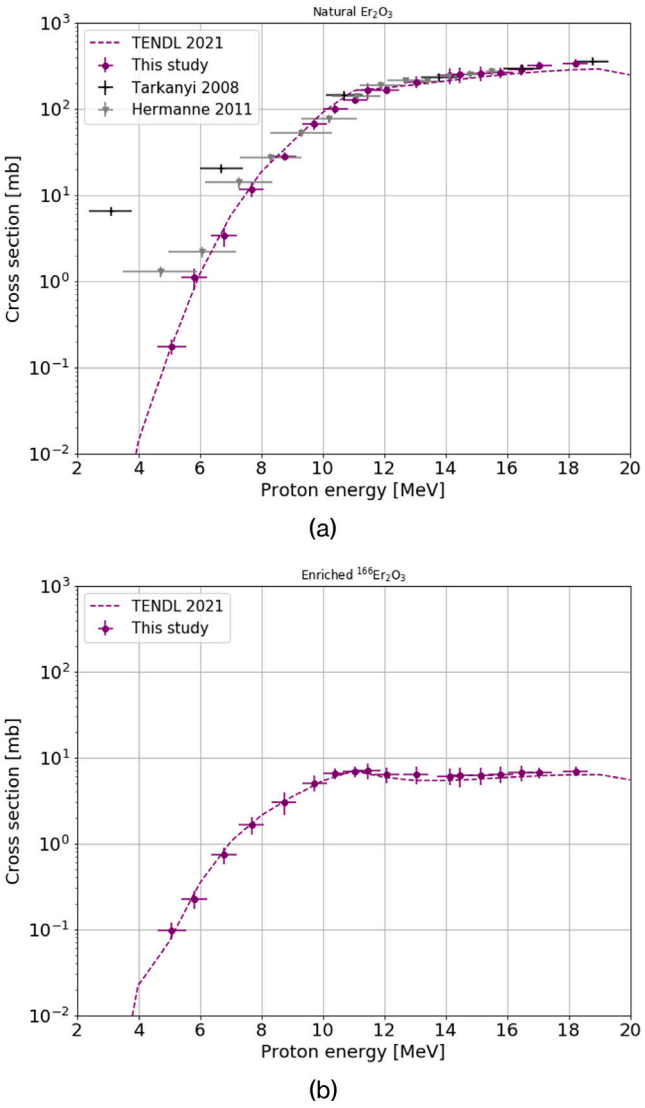

Fig. 6. ^{167}Tm production cross section from natural Er_2O_3 (a) and enriched $^{166}Er_2O_3$ (b), whose isotopic composition is reported in Table 2.

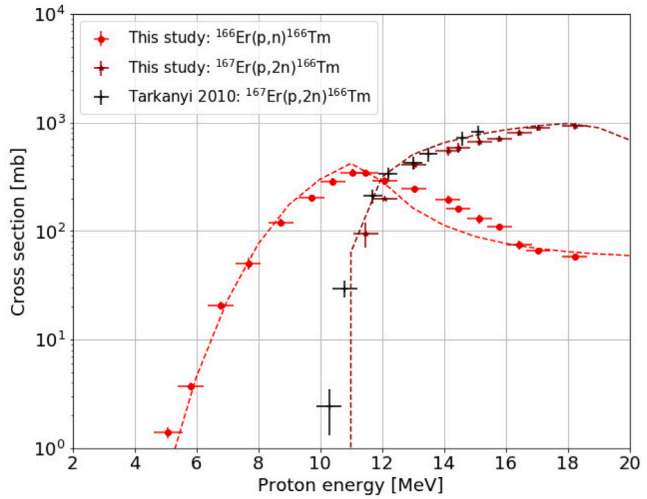

Fig. 5. ^{166}Er(p,n)^{166}Tm and ^{167}Er(p,2n)^{166}Tm nuclear cross sections. The dots are the experimental data, the dashed lines are the TENDL calculations.

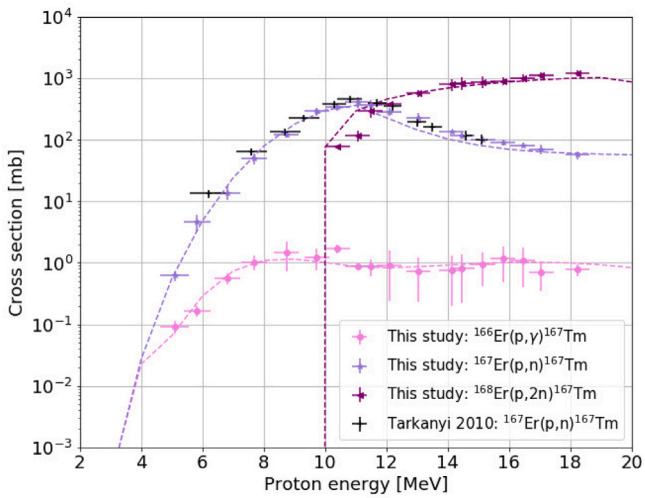

Fig. 7. ^{166}Er(p, γ)^{167}Tm, ^{167}Er(p,n)^{167}Tm and ^{168}Er(p,2n)^{167}Tm nuclear cross sections. The dots are the experimental data, the dashed lines are the TENDL calculations.

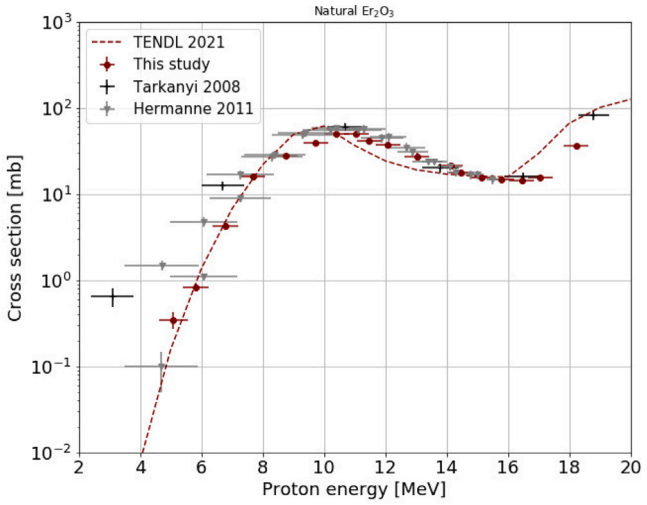

Fig. 8. ^{168}Tm production cross section from natural Er_2O_3.

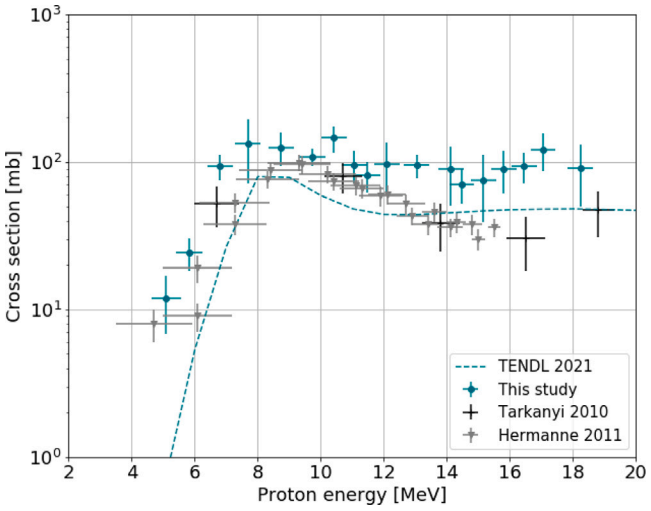

Fig. 10. ^{170}Er(p,n)^{170}Tm nuclear cross sections.

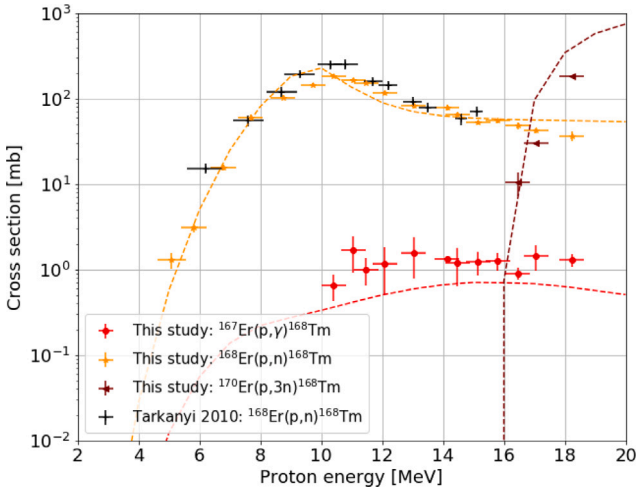

Fig. 9. ^{167}Er(p, γ)^{168}Tm, ^{168}Er(p,n)^{168}Tm and ^{170}Er(p,3n)^{168}Tm nuclear cross sections. The dots are the experimental data, the dashed lines are the TENDL calculations.

(2010) for the ^{168}Er(p,n)^{168}Tm reaction, showing a good agreement. The cross sections of the other two reactions are measured here for the first time.

The numerical data are reported in the Appendix (Tables 5 and 10) for completeness.

Thulium-170. In the energy range of interest, ^{170}Tm is only produced via the reaction ^{170}Er(p,n)^{170}Tm. The cross sections measured from natural Er_2O_3 are reported in Fig. 10 and compared with TENDL-2021 predictions (Koning and Rochman, 2012) as well as the findings reported by Tárkányi et al. (2010) and Hermanne et al. (2011). A reasonable agreement was found with the experimental data for energies below 12 MeV, while at higher energies some discrepancies are observed. TENDL predictions seem to underestimate the experimental data over the entire energy range.

In the case of enriched $^{166}Er_2O_3$, ^{170}Tm could not be measured due to the low isotopic percentage of ^{170}Er.

The numerical data are reported in the Appendix (Table 11) for completeness.

3.2. Study of the production yield and purity

On the basis of the results obtained, a study of the Thick Target Yield (TTY) and purity was performed to optimize ^{165}Er production.

From the cross-section measurements, the TTY for a given proton impinging energy, E, can be calculated using the following formula:

$$TTY(E,t_i) = \frac{A(t_i)}{I} = (1 - e^{-\lambda \cdot t_i}) \cdot \frac{N_A \cdot \eta}{m_{mol} \cdot q} \int_{E_{th}}^{E} \frac{\sigma(E')}{S_p(E')} dE' \quad (2)$$

where t_i is the irradiation time, I the current on target, $A(t_i)$ the activity produced at EoB, λ the decay constant, $\sigma(E')$ the cross section as a function of the proton kinetic energy E', $S_p(E')$ is the mass stopping power for the target material, E_{th} is the threshold energy of the considered reaction, N_A the Avogadro constant, m_{mol} the average molar mass of the target material, η the number of target atoms of the desired species per molecule and q the charge of the projectile. The mass stopping power was calculated using SRIM.

Given a sample containing a mixture of N radioisotopes, the purity of the radionuclide of interest X is given by

$$P_X = \frac{A_X}{\sum_i^N A_i} \quad (3)$$

where A_i is the activity of the ith radionuclide.

If a thin target is used, such that the range of the proton beam is shorter than the target thickness, the production yield, Y(E), can be defined as

$$Y(E) = TTY(E) - TTY(E_{out}) \quad (4)$$

where E_{out} is the proton energy after the target, calculated by using SRIM.

From the results of the cross-section measurements, it can be observed that the highest production yield and purity can be achieved for the maximum obtainable energy. With an 18 MeV medical cyclotron equipped with a solid target station, a maximum energy of about 17.8 MeV is achievable by employing a commercial Havar window foil of ~10 μm.

Having fixed the input energy at this value, the purity depends strongly on the output energy and, thus, on the target thickness, due to the increase in the ^{166}Tm cross section until it peaks at about 11 MeV. From Fig. 11 it can be seen that the purity is virtually stable for target thicknesses up to about 180 μm. However, it has been observed that the pellets must be at least 240-μm thick to be robust enough to be handled. This leads to an output energy of 15.9 MeV. Since ^{166}Tm has a shorter half-life than ^{165}Tm, longer irradiation times can be

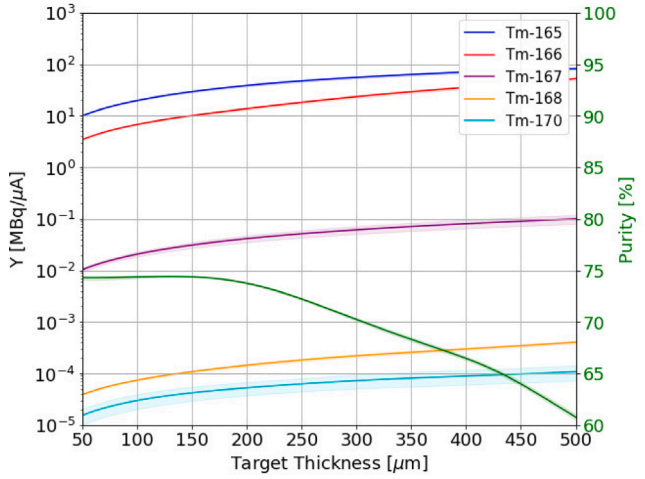

Fig. 11. Tm radioisotope yields and radionuclidic purity (indicated by the green line) as a function of the target thickness, for an input energy of 17.8 MeV and 1-h irradiation. The bands correspond to the maximum and minimum yield calculated on the basis of the measured cross sections.

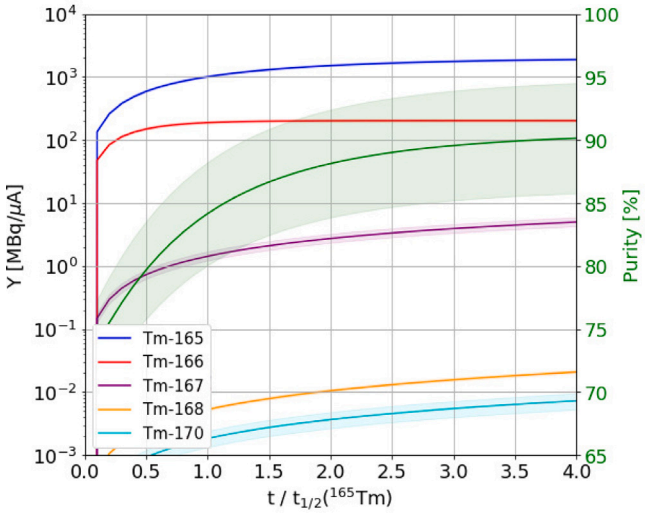

Fig. 12. Tm radioisotope yields and radionuclidic purity (indicated by the green line) as a function of the irradiation time, considering the energy range 17.8–15.9 MeV. The bands correspond to the maximum and minimum yield calculated on the basis of the measured cross sections.

considered to improve radionuclidic purity. In this case, however, the long-lived Tm impurities must be kept under control. The production yield of Tm radioisotopes and the radionuclidic purity were studied as a function of irradiation time in the energy range 17.8–15.9 MeV (Fig. 12). Considering an irradiation time of 30 h, a ^{165}Tm production yield of about 1 GBq/μA with a radionuclidic purity of 84% can be achieved according to our findings. ^{166}Tm is the main impurity in the sample, accounting for about 15.7%.

It is important to underline that all thulium impurities decay into stable isotopes of Er. Thus, the product ^{165}Er formed by the decay is not carrier-free but contains small amounts of isotopic carriers. To ensure a high purity of the eluted ^{165}Er, it is necessary to determine the best time

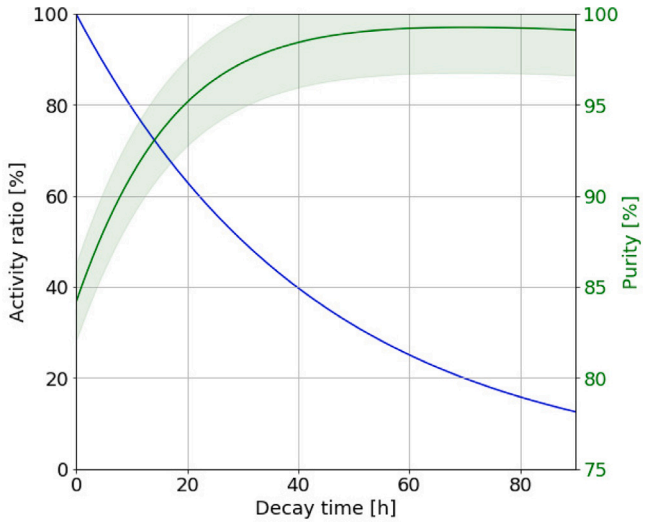

Fig. 13. ^{165}Tm activity ratio and radionuclidic purity as a function of the decay time, considering an irradiation time of 30 h in the energy range 17.8–15.9 MeV. The bands correspond to the maximum and minimum yield calculated on the basis of the measured cross sections.

to perform the chemical separation and fix the Tm parent radioisotopes on the generator column.

A decay time of about 30 h results in a radionuclidic purity of more than 97%, retaining 50% of the produced ^{165}Tm activity (Fig. 13). Considering a ^{165}Er in-growth time of 1.012 d, as suggested by Tárkányi et al. (2009), it is possible to obtain 289 MBq/μA of ^{165}Er, corresponding to a specific activity of 11 $\cdot 10^3$ TBq/μA.mmol$_{Er}$, under the assumption of a 100% efficiency of the chemical separation and elution procedures.

The effective purity of the solution depends on the actual efficiency of the separation and elution processes, not easy in the case of lanthanides.

As the ^{165}Tm cross section was found to increase at 18 MeV, the use of higher energies (e.g. 24 MeV) can be evaluated to improve this result.

3.3. Production tests

On the basis of the results obtained on yield and purity, the optimal conditions for the production of ^{165}Tm were assessed. The production tests were carried out in the BTL to evaluate the cross-section measurements in the energy range of interest.

In order not to degrade the energy of the beam, the pellet was placed in a coin with a 7-mm-diameter hole in the front part (Fig. 14). A 13-μm-thick aluminum foil was placed inside the coin to prevent the material from escaping during the irradiation. This configuration results in an input energy of (18.2 ± 0.4) MeV.

Two enriched $^{166}Er_2O_3$ pellets, 0.24-mm and 0.46-mm thick, were irradiated in order to verify the impact of the target thickness on radionuclidic purity.

The irradiation parameters and the experimental results are reported in Table 4. A good agreement with the prediction based on cross-section measurements was found (Fig. 15).

4. Conclusions and outlook

^{165}Er is a radionuclide with promising characteristics for targeted radionuclide therapy using Auger electrons. Its indirect production via the ^{166}Er(p,2n)^{165}Tm → ^{165}Er reaction was investigated at the Bern medical cyclotron by irradiating enriched $^{166}Er_2O_3$ solid targets. Despite the use of highly enriched target material, several Tm impurities

Table 4
Irradiation parameters, ^{165}Tm yield and radionuclidic purity EoB, obtained irradiating 91.9% enriched $^{166}Er_2O_3$ pellets. *I* is the average current hitting the 6-mm-diameter pellet. The values in parentheses are the yield calculations based on the cross-section measurements.

Irradiation [#]	Δx pellet [μm]	E_{in} [MeV]	t_{irr} [h]	I [nA]	Y(^{165}Tm) [MBq/μA]	P(EoB) [%]
1	0.49 ± 0.01	18.2 ± 0.4	0.253 ± 0.003	3.42 ± 0.08	90 ± 6 *(86)*	67 ± 2 *(67)*
2	0.24 ± 0.01	18.2 ± 0.4	0.195 ± 0.002	4.9 ± 0.1	46 ± 3 *(47)*	74 ± 2 *(75)*

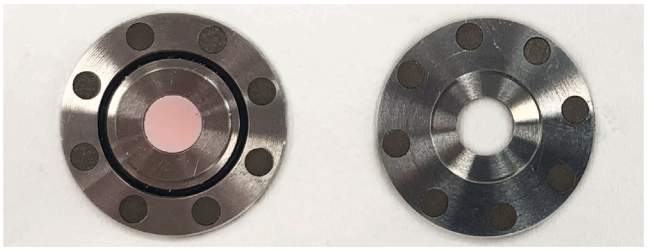

Fig. 14. Coin with a 7-mm-diameter hole in the covering lid, containing an enriched $^{166}Er_2O_3$ pellet.

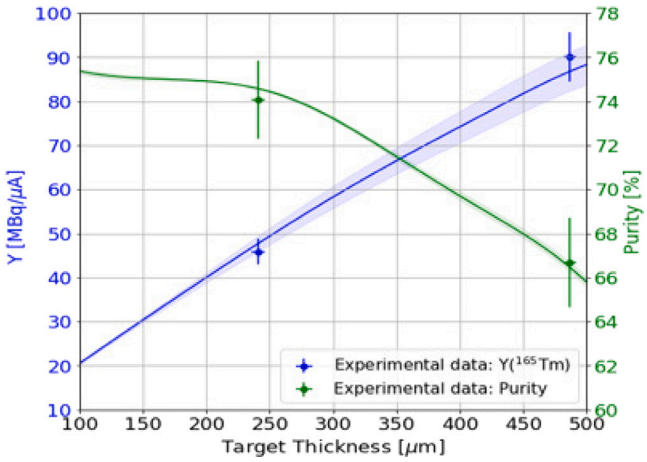

Fig. 15. ^{165}Tm production yield and purity calculated in our irradiation conditions compared to the experimental results, considering 1-h irradiation. The bands correspond to the maximum and minimum yield derived from the measured cross sections.

are produced during irradiation, making precise knowledge of cross sections necessary to optimize the production yield and the radionuclidic purity. Using a method developed by LHEP, it was possible to determine the cross sections of all nuclear reactions producing Tm radioisotopes in the energy range of the medical cyclotron. To the best of our knowledge, prior to this work no experimental data were available for the reactions ^{164}Er(p, γ)^{165}Tm, ^{166}Er(p,n)^{166}Tm, ^{166}Er(p, γ)^{167}Tm, ^{167}Er(p,3n)^{165}Tm, ^{167}Er(p, γ)^{168}Tm, ^{168}Er(p,2n)^{167}Tm and ^{170}Er(p,3n)^{168}Tm.

A study of the production yield and radionuclidic purity was carried out on the basis of the measured cross section to determine the optimal irradiation conditions. Two production tests were performed in the Beam Transport Line (BTL) to assess the correctness of these calculations.

When considering a proton entry energy of 17.8 MeV, an irradiation time of 30 h and a 240-μm 98.1% enriched $^{166}Er_2O_3$ target (Table 2), about 1 GBq/μA of ^{165}Tm can be achieved at EoB, that leads to 289 MBq/μA of ^{165}Er, assuming a decay time of about 30 h before the first chemical separation and an in-growth time of ~1 d. This result corresponds to a ^{165}Er specific activity of 11 $\cdot 10^3$ TBq/μA.mmol$_{Er}$, in agreement with that reported by Tárkányi et al. (2009). It is important to remark that this estimation was made assuming a chemical separation yield of 100%. However, these chemical processes are particularly complicated in the case of lanthanides and need to be further investigated.

According to our findings (Gracheva et al., 2020), the direct ^{165}Ho(p,n)^{165}Er nuclear reaction is the most productive in the energy range of a medical cyclotron. Nevertheless, since the cross section of the ^{166}Er(p,2n)^{165}Tm reaction was found to be increasing at 18 MeV, the use of cyclotrons with higher proton energy can be evaluated to achieve higher production yields.

CRediT authorship contribution statement

Gaia Dellepiane: Writing – original draft, Visualization, Validation, Software, Methodology, Investigation, Formal analysis, Data curation, Conceptualization. **Pierluigi Casolaro:** Writing – review & editing, Investigation. **Chiara Favaretto:** Writing – review & editing, Investigation. **Alexander Gottstein:** Writing – review & editing, Investigation. **Pascal V. Grundler:** Writing – review & editing, Investigation. **Isidre Mateu:** Writing – review & editing, Investigation. **Edoardo Renaldin:** Writing – review & editing, Methodology, Investigation, Data curation. **Paola Scampoli:** Writing – review & editing, Investigation, Conceptualization. **Zeynep Talip:** Writing – review & editing, Supervision, Investigation, Funding acquisition, Conceptualization. **Nicholas P. van der Meulen:** Writing – review & editing, Supervision, Investigation, Funding acquisition, Conceptualization. **Saverio Braccini:** Writing – review & editing, Supervision, Resources, Project administration, Methodology, Investigation, Funding acquisition, Conceptualization.

Declaration of competing interest

The authors declare the following financial interests/personal relationships which may be considered as potential competing interests: Saverio Braccini, Zeynep Talip, Nicholas P. van der Meulen reports financial support was provided by Swiss National Science Foundation.

Data availability

Data will be made available on request.

Acknowledgments

We acknowledge contributions from LHEP engineering and technical staff (Roger Hänni and Jan Christen, in particular) and from the SWAN Isotopen AG team (Riccardo Bosi and Michel Eggemann, in particular). This research project was partially funded by the Swiss National Science Foundation (SNSF) (grants: CRSII5_175749 and 200021_188495).

Appendix

See Tables 5–11.

Table 5
^{165}Tm,^{166}Tm,^{167}Tm and^{168}Tm production cross-section data measured from natural Er_2O_3.

E [MeV]	$\sigma(^{165}Tm)$ [mbarn]	$\sigma(^{166}Tm)$ [mbarn]	$\sigma(^{167}Tm)$ [mbarn]	$\sigma(^{168}Tm)$ [mbarn]
5.1 ± 0.5	Not detected	0.19 ± 0.03	0.17 ± 0.03	0.35 ± 0.08
5.8 ± 0.4	0.03 ± 0.01	0.77 ± 0.08	1.1 ± 0.3	0.83 ± 0.09
6.8 ± 0.4	Not detected	3.7 ± 0.4	3.4 ± 0.8	4.2 ± 0.3
7.7 ± 0.4	0.12 ± 0.02	12 ± 1	11.7 ± 2.4	16 ± 1
8.7 ± 0.4	0.15 ± 0.02	26 ± 1	28 ± 3	28 ± 2
9.7 ± 0.4	0.14 ± 0.02	56 ± 4	67 ± 10	39 ± 2
10.4 ± 0.4	0.43 ± 0.08	80 ± 5	99 ± 12	50 ± 2
11.1 ± 0.4	2.8 ± 0.3	104 ± 9	126 ± 13	50 ± 2
11.5 ± 0.4	22 ± 2	138 ± 13	163 ± 34	41 ± 3
12.1 ± 0.4	30 ± 2	143 ± 9	167 ± 18	37 ± 1
13.0 ± 0.4	88 ± 5	175 ± 12	206 ± 31	27 ± 3
14.1 ± 0.4	169 ± 14	190 ± 16	245 ± 50	21 ± 2
14.5 ± 0.4	204 ± 18	188 ± 17	253 ± 54	18 ± 1
15.2 ± 0.4	233 ± 19	195 ± 17	260 ± 53	15.4 ± 0.9
15.8 ± 0.4	243 ± 14	197 ± 12	264 ± 39	15.0 ± 0.9
16.5 ± 0.4	276 ± 16	209 ± 13	289 ± 42	14.5 ± 0.8
17.1 ± 0.4	307 ± 16	226 ± 15	319 ± 33	15.7 ± 0.8
18.2 ± 0.4	341 ± 19	231 ± 16	338 ± 36	37 ± 1

Table 6
^{165}Tm,^{166}Tm and^{167}Tm production cross-section data measured from the 98.1% enriched$^{166}Er_2O_3$ material, whose isotopic composition is reported in Table 2.

E [MeV]	$\sigma(^{165}Tm)$ [mbarn]	$\sigma(^{166}Tm)$ [mbarn]	$\sigma(^{167}Tm)$ [mbarn]
5.1 ± 0.5	Not detected	1.4 ± 0.2	0.10 ± 0.02
5.8 ± 0.4	Not detected	3.6 ± 0.3	0.23 ± 0.05
6.8 ± 0.4	Not detected	20 ± 2	0.7 ± 0.2
7.7 ± 0.4	Not detected	49 ± 6	1.7 ± 0.4
8.7 ± 0.4	Not detected	118 ± 10	3.1 ± 0.9
9.7 ± 0.4	Not detected	199 ± 12	5 ± 1
10.4 ± 0.4	0.9 ± 0.1	282 ± 24	6.5 ± 0.9
11.1 ± 0.4	21 ± 1	337 ± 29	7 ± 1
11.5 ± 0.4	55 ± 3	341 ± 21	7 ± 2
12.1 ± 0.4	206 ± 17	288 ± 25	6 ± 1
13.0 ± 0.4	342 ± 20	246 ± 15	6 ± 1
14.1 ± 0.4	458 ± 38	198 ± 17	6 ± 1
14.5 ± 0.4	606 ± 35	166 ± 10	6 ± 2
15.2 ± 0.4	667 ± 54	136 ± 12	6 ± 1
15.8 ± 0.4	737 ± 42	117 ± 7	6 ± 1
16.5 ± 0.4	819 ± 66	83 ± 8	7 ± 1
17.1 ± 0.4	853 ± 40	77 ± 4	7 ± 1
18.2 ± 0.4	950 ± 44	69 ± 4	6.9 ± 0.9

Table 7
^{164}Er(p, γ)^{165}Tm,^{166}Er(p,2n)^{165}Tm and^{167}Er(p,3n)^{165}Tm nuclear cross-section data.

E [MeV]	^{164}Er(p, γ)^{165}Tm [mbarn]	^{166}Er(p,2n)^{165}Tm [mbarn]	^{167}Er(p,3n)^{165}Tm [mbarn]
5.8 ± 0.4	1.8 ± 0.4	Not detected	Not detected
7.7 ± 0.4	7 ± 1	Not detected	Not detected
8.7 ± 0.4	9 ± 1	Not detected	Not Detected
9.7 ± 0.4	9 ± 1	Not detected	Not Detected
10.4 ± 0.4	8 ± 3	0.9 ± 0.1	Not Detected
11.1 ± 0.4	Not Detected	21 ± 1	Not Detected
11.5 ± 0.4	Not Detected	56 ± 3	Not Detected
12.1 ± 0.4	Not Detected	210 ± 18	Not Detected
13.0 ± 0.4	Not Detected	349 ± 20	Not Detected
14.1 ± 0.4	Not Detected	467 ± 38	Not Detected
14.5 ± 0.4	Not Detected	618 ± 35	Not Detected
15.2 ± 0.4	Not Detected	680 ± 55	Not Detected
15.8 ± 0.4	Not Detected	752 ± 43	Not Detected
16.5 ± 0.4	Not Detected	835 ± 68	Not Detected
17.1 ± 0.4	Not Detected	870 ± 41	Not Detected
18.2 ± 0.4	Not Detected	1005 ± 56	18 ± 1

Table 8
^{166}Er(p,n)^{166}Tm and^{167}Er(p,2n)^{166}Tm nuclear cross-section data.

E [MeV]	^{166}Er(p,n)^{166}Tm [mbarn]	^{167}Er(p,2n)^{166}Tm [mbarn]
5.1 ± 0.5	1.4 ± 0.2	Not Detected
5.8 ± 0.4	3.7 ± 0.3	Not Detected
6.8 ± 0.4	21 ± 2	Not Detected
7.7 ± 0.4	50 ± 6	Not Detected
8.7 ± 0.4	120 ± 11	Not Detected
9.7 ± 0.4	203 ± 13	Not Detected
10.4 ± 0.4	287 ± 25	Not Detected
11.1 ± 0.4	343 ± 30	Not Detected
11.5 ± 0.4	346 ± 21	95 ± 25
12.1 ± 0.4	290 ± 26	200 ± 14
13.0 ± 0.4	245 ± 15	408 ± 30
14.1 ± 0.4	194 ± 17	545 ± 47
14.5 ± 0.4	161 ± 10	588 ± 62
15.2 ± 0.4	129 ± 11	664 ± 57
15.8 ± 0.4	109 ± 7	703 ± 45
16.5 ± 0.4	74 ± 7	805 ± 45
17.1 ± 0.4	66 ± 3	892 ± 60
18.2 ± 0.4	58 ± 4	925 ± 63

Table 9
^{166}Er(p, γ)^{167}Tm,^{167}Er(p,n)^{167}Tm and^{168}Er(p,2n)^{167}Tm nuclear cross-section data.

E [MeV]	^{166}Er(p, γ)^{167}Tm [mbarn]	^{167}Er(p,n)^{167}Tm [mbarn]	^{168}Er(p,2n)^{167}Tm [mbarn]
5.1 ± 0.5	0.09 ± 0.02	0.6 ± 0.1	Not Detected
5.8 ± 0.4	0.17 ± 0.03	5 ± 1	Not Detected
6.8 ± 0.4	0.6 ± 0.1	14 ± 4	Not Detected
7.7 ± 0.4	1.0 ± 0.3	50 ± 10	Not Detected
8.7 ± 0.4	1.5 ± 0.7	122 ± 12	Not Detected
9.7 ± 0.4	1.2 ± 0.5	290 ± 44	Not Detected
10.4 ± 0.4	1.7 ± 0.3	339 ± 49	77 ± 1
11.1 ± 0.4	0.9 ± 0.3	411 ± 84	116 ± 24
11.5 ± 0.4	0.9 ± 0.3	366 ± 74	293 ± 62
12.1 ± 0.4	0.9 ± 0.7	285 ± 43	375 ± 28
13.0 ± 0.4	0.7 ± 0.5	226 ± 47	571 ± 73
14.1 ± 0.4	0.8 ± 0.6	133 ± 2	794 ± 186
14.5 ± 0.4	0.8 ± 0.6	117 ± 13	838 ± 189
15.2 ± 0.4	0.9 ± 0.5	100 ± 10	878 ± 188
15.8 ± 0.4	1.2 ± 0.7	90 ± 10	899 ± 134
16.5 ± 0.4	1.1 ± 0.7	82 ± 8	1000 ± 146
17.1 ± 0.4	0.7 ± 0.3	70 ± 13	1121 ± 111
18.2 ± 0.4	0.8 ± 0.2	57 ± 8	1204 ± 127

Table 10
^{167}Er(p, γ)^{168}Tm,^{168}Er(p,n)^{168}Tm and^{170}Er(p,3n)^{168}Tm nuclear cross-section data.

E [MeV]	^{167}Er(p, γ)^{168}Tm [mbarn]	^{168}Er(p,n)^{168}Tm [mbarn]	^{170}Er(p,3n)^{168}Tm [mbarn]
5.1 ± 0.5	Not Detected	1.3 ± 0.3	Not Detected
5.8 ± 0.4	Not Detected	3.1 ± 0.4	Not Detected
6.8 ± 0.4	Not Detected	16 ± 1	Not Detected
7.7 ± 0.4	Not Detected	60 ± 5	Not Detected
8.7 ± 0.4	Not Detected	103 ± 7	Not Detected
9.7 ± 0.4	Not Detected	145 ± 7	Not Detected
10.4 ± 0.4	0.7 ± 0.2	184 ± 7	Not Detected
11.1 ± 0.4	1.7 ± 0.8	166 ± 6	Not Detected
11.5 ± 0.4	1.0 ± 0.4	153 ± 10	Not Detected
12.1 ± 0.4	1.2 ± 0.7	118 ± 4	Not Detected
13.0 ± 0.4	1.6 ± 0.8	82 ± 5	Not Detected
14.1 ± 0.4	1.3 ± 0.1	79 ± 6	Not Detected
14.5 ± 0.4	1.2 ± 0.6	65 ± 4	Not Detected
15.2 ± 0.4	1.2 ± 0.4	53 ± 2	Not Detected
15.8 ± 0.4	1.3 ± 0.3	55 ± 3	Not Detected
16.5 ± 0.4	0.9 ± 0.1	49 ± 5	10 ± 3
17.1 ± 0.4	1.5 ± 0.5	43 ± 3	30 ± 1
18.2 ± 0.4	1.3 ± 0.2	37 ± 5	185 ± 2

Table 11
$^{170}Er(p,n)^{170}Tm$ nuclear cross-section data measured from natural Er_2O_3.

E [MeV]	$^{170}Er(p,n)^{170}Tm$ [mbarn]
5.1 ± 0.5	12 ± 5
5.8 ± 0.4	24 ± 6
6.8 ± 0.4	93 ± 19
7.7 ± 0.4	133 ± 62
8.7 ± 0.4	126 ± 32
9.7 ± 0.4	108 ± 15
10.4 ± 0.4	145 ± 30
11.1 ± 0.4	95 ± 23
11.5 ± 0.4	81 ± 19
12.1 ± 0.4	97 ± 38
13.0 ± 0.4	95 ± 17
14.1 ± 0.4	89 ± 38
14.5 ± 0.4	70 ± 19
15.2 ± 0.4	75 ± 36
15.8 ± 0.4	90 ± 29
16.5 ± 0.4	93 ± 22
17.1 ± 0.4	121 ± 34
18.2 ± 0.4	91 ± 41

References

Abriola, D., Verpelli, M., 2011. Information management tools for evaluated nuclear structure data file (ENSDF) interrogation and dissemination. J. Korean Phys. Soc. 59 (2), 1322–1324. http://dx.doi.org/10.3938/jkps.59.1322.

Auger, M., Braccini, S., Carzaniga, T.S., Ereditato, A., Nesteruk, K.P., Scampoli, P., 2016. A detector based on silica fibers for ion beam monitoring in a wide current range. J. Instrum. 11 (03), P03027. http://dx.doi.org/10.1088/1748-0221/11/03/p03027.

Auger, M., Braccini, S., Ereditato, A., Nesteruk, K.P., Scampoli, P., 2015. Low current performance of the Bern medical cyclotron down to the pA range. Meas. Sci. Technol. 26, http://dx.doi.org/10.1088/0957-0233/26/9/094006.

Baglin, C.M., 2000. Nuclear data sheets for A=167. Nucl. Data Sheets 90 (3), 431–644. http://dx.doi.org/10.1006/ndsh.2000.0012.

Baglin, C.M., 2008. Nuclear data sheets for A=166. Nucl. Data Sheets 109 (5), 1103–1382. http://dx.doi.org/10.1016/j.nds.2008.04.001.

Baglin, C.M., 2010. Nuclear data sheets for A=168. Nucl. Data Sheets 111 (7), 1807–2080. http://dx.doi.org/10.1016/j.nds.2010.07.001.

Baglin, C., McCutchan, E., Basunia, S., Browne, E., 2018. Nuclear data sheets for A=170. Nucl. Data Sheets 153, 1–494. http://dx.doi.org/10.1016/j.nds.2018.11.001.

Beyer, G., Zeisler, S., Becker, D., 2004. The Auger-electron emitter ^{165}Er: excitation function of the ^{165}Ho(p, n)^{165}Er process. Radiochim. Acta 92 (4–6), 219–222. http://dx.doi.org/10.4236/jmp.2010.14033.

Braccini, S., 2013. The new Bern PET cyclotron, its research beam line, and the development of an innovative beam monitor detector. AIP Conf. Proc. 1525, 144–150. http://dx.doi.org/10.1063/1.4802308.

Braccini, S., Carzaniga, T.S., Dellepiane, G., Grundler, P.V., Scampoli, P., van der Meulen, N.P., Wüthrich, D., 2022. Optimization of ^{68}Ga production at an 18 MeV medical cyclotron with solid targets by means of cross-section measurement of ^{66}Ga, ^{67}Ga and ^{68}Ga. Appl. Radiat. Isot. 110252. http://dx.doi.org/10.1016/j.apradiso.2022.110252.

Braccini, S., Scampoli, P., 2016. Science with a medical cyclotron. CERN Cour. 21–22.

Carzaniga, T.S., Auger, M., Braccini, S., Bunka, M., Ereditato, A., Nesteruk, K.P., Scampoli, P., Türler, A., 2017. Measurement of ^{43}Sc and ^{44}Sc production cross-section with an 18 MeV medical PET cyclotron. Appl. Radiat. Isot. (ISSN: 0969-8043) 129, 96–102. http://dx.doi.org/10.1016/j.apradiso.2017.08.013.

Cotton, S., 2006. Coordination chemistry of the lanthanides. In: Lanthanide and Actinide Chemistry. John Wiley & Sons, Ltd, ISBN: 9780470010082, pp. 35–60. http://dx.doi.org/10.1002/0470010088.ch4.

Dellepiane, G., Belver Aguilar, C., Carzaniga, T.S., Casolaro, P., Häffner, P., Scampoli, P., Schmid, M., Braccini, S., 2021. Research on theranostic radioisotope production at the Bern medical cyclotron. IL NUOVO CIMENTO C 44, http://dx.doi.org/10.1393/ncc/i2021-21130-6.

Dellepiane, G., Casolaro, P., Favaretto, C., Grundler, P.V., Mateu, I., Scampoli, P., Talip, Z., van der Meulen, N.P., Braccini, S., 2022a. Cross section measurement of terbium radioisotopes for an optimized ^{155}Tb production with an 18 MeV medical PET cyclotron. Appl. Radiat. Isot. (ISSN: 0969-8043) 184, 110175. http://dx.doi.org/10.1016/j.apradiso.2022.110175.

Dellepiane, G., Casolaro, P., Gottstein, A., Mateu, I., Scampoli, P., Braccini, S., 2023. Optimized production of ^{67}Cu based on cross section measurements of ^{67}Cu and ^{64}Cu using an 18 MeV medical cyclotron. Appl. Radiat. Isot. (ISSN: 0969-8043) 195, 110737. http://dx.doi.org/10.1016/j.apradiso.2023.110737.

Dellepiane, G., Casolaro, P., Mateu, I., Scampoli, P., Braccini, S., 2022b. Alternative routes for ^{64}Cu production using an 18 MeV medical cyclotron in view of theranostic applications. Appl. Radiat. Isot. (ISSN: 0969-8043) 110518. http://dx.doi.org/10.1016/j.apradiso.2022.110518.

Dellepiane, G., Casolaro, P., Mateu, I., Scampoli, P., Voeten, N., Braccini, S., 2022c. ^{47}Sc and ^{46}Sc cross-section measurement for an optimized ^{47}Sc production with an 18 MeV medical PET cyclotron. Appl. Radiat. Isot. (ISSN: 1872-9800) 189, 110428. http://dx.doi.org/10.1016/j.apradiso.2022.110428.

Dellepiane, G., Casolaro, P., Mateu, I., Scampoli, P., Voeten, N., Braccini, S., 2022d. Cross-section measurement for an optimized ^{61}Cu production at an 18 MeV medical cyclotron from natural Zn and enriched ^{64}Zn solid targets. Appl. Radiat. Isot. 190, 110466. http://dx.doi.org/10.1016/j.apradiso.2022.110466.

Durán, M.T., Juget, F., Nedjadi, Y., Bailat, C., Grundler, P.V., Talip, Z., van der Meulen, N.P., Casolaro, P., Dellepiane, G., Braccini, S., 2022. Half-life measurement of ^{44}Sc and ^{44m}Sc. Appl. Radiat. Isot. 190, 110507. http://dx.doi.org/10.1016/j.apradiso.2022.110507.

Falzone, N., Cornelissen, B., Vallis, K.A., 2012. Auger emitting radiopharmaceuticals for cancer therapy. In: García Gómez-Tejedor, G., Fuss, M.C. (Eds.), Radiation Damage in Biomolecular Systems. Springer Netherlands, Dordrecht, ISBN: 978-94-007-2564-5, pp. 461–478. http://dx.doi.org/10.1007/978-94-007-2564-5_28.

Favaretto, C., Talip, Z., Borgna, F., Grundler, P.V., Dellepiane, G., Sommerhalder, A., Zhang, H., Schibli, R., Braccini, S., Müller, C., van der Meulen, N.P., 2021. Cyclotron production and radiochemical purification of terbium-155 for SPECT imaging. EJNMMI Radiopharm. Chem. 6, 37. http://dx.doi.org/10.1186/s41181-021-00153-w.

Forgács, A., Balkay, L., Trón, L., Raics, P., 2014. Excel2Genie: A microsoft excel application to improve the flexibility of the genie-2000 spectroscopic software. Appl. Radiat. Isot. 94, 77–81. http://dx.doi.org/10.1016/j.apradiso.2014.07.005.

Gracheva, N., Carzaniga, T., Schibli, R., Braccini, S., van der Meulen, N., 2020. ^{165}Er: A new candidate for Auger electron therapy and its possible cyclotron production from natural holmium targets. Appl. Radiat. Isot. 159, 109079. http://dx.doi.org/10.1016/j.apradiso.2020.109079.

Häffner, P.D., Aguilar, C.B., Braccini, S., Scampoli, P., Thonet, P.A., 2019. Study of the extracted beam energy as a function of operational parameters of a medical cyclotron. Instruments 3 (63), http://dx.doi.org/10.3390/instruments3040063.

Herman, M., Capote, R., Carlson, B., Obložinský, P., Sin, M., Trkov, A., Wienke, H., Zerkin, V., 2007. EMPIRE: Nuclear reaction model code system for data evaluation. Nucl. Data Sheets (ISSN: 0090-3752) 108 (12), 2655–2715. http://dx.doi.org/10.1016/j.nds.2007.11.003, Special Issue on Evaluations of Neutron Cross Sections.

Hermanne, A., Adam-Rebeles, R., Tárkányi, F., Takács, S., Csikai, J., Takács, M., Ignatyuk, A., 2013. Deuteron induced reactions on Ho and La: Experimental excitation functions and comparison with code results. Nucl. Instrum. Methods Phys. Res. B 311, 102–111. http://dx.doi.org/10.1016/j.nimb.2013.06.014.

Hermanne, A., Rebeles, R.A., Tárkányi, F., Takács, S., Kiraly, B., Ignatyuk, A.V., 2011. Cross sections for production of longer lived ^{170,168,167}Tm in 16 MeV proton irradiation of ^{nat}Er. Nucl. Instrum. Methods Phys. Res. B 269 (7), 695–699. http://dx.doi.org/10.1016/j.nimb.2011.01.130.

International Standard, 2021. Nuclear Instrumentation – Measurement of Activity Or Emission Rate of Gamma-Ray Emitting Radionuclides – Calibration and Use of Germanium-Based Spectrometers. ISBN: 978-2-8322-9813-8, IEC 61452:2021.

Isoflex, 2022. Isotope for science, medicine and industry. URL http://www.isoflex.com/. (Last access 14 October 2022).

Jain, A.K., Ghosh, A., Singh, B., 2006. Nuclear data sheets for A=165. Nucl. Data Sheets 107 (5), 1075–1346. http://dx.doi.org/10.1016/j.nds.2006.05.002.

Juget, F., Durán, M.T., Nedjadi, Y., Talip, Z., Grundler, P.V., Favaretto, C., Casolaro, P., Dellepiane, G., Braccini, S., Bailat, C., van der Meulen, N.P., 2023. Activity measurement of ^{44}Sc and calibration of activity measurement instruments on production sites and clinics. Molecules 28, 1345. http://dx.doi.org/10.3390/molecules28031345.

Kassis, A., 2004. The amazing world of auger electrons. Int. J. Radiat. Biol. 80 (11–12), 789–803. http://dx.doi.org/10.1080/09553000400017663.

Kassis, A.I., Adelstein, S.J., 2005. Radiobiologic principles in radionuclide therapy. J. Nucl. Med. (ISSN: 0161-5505) 46 (1), 4–12.

Koning, A., Rochman, D., 2012. Modern nuclear data evaluation with the TALYS code system. Nucl. Data Sheets 113, 2841–2934. http://dx.doi.org/10.1016/j.nds.2012.11.002.

Ku, A., Facca, V.J., Cai, Z., Reilly, R.M., 2019. Auger electrons for cancer therapy – a review. EJNMMI Radiopharm. Chem. 4, http://dx.doi.org/10.1186/s41181-019-0075-2.

Meija, J., Coplen, T.B., Berglund, M., Brand, W.A., Bièvre, P.D., Gröning, M., Holden, N.E., Irrgeher, J., Loss, R.D., Walczyk, T., Prohaska, T., 2016. Isotopic compositions of the elements 2013 (IUPAC technical report). Pure Appl. Chem. 88 (3), 293–306. http://dx.doi.org/10.1515/pac-2015-0503.

van der Meulen, N.P., Hasler, R., Talip, Z., Grundler, P.V., Favaretto, C., Umbricht, C.A., Müller, C., Dellepiane, G., Carzaniga, T.S., Braccini, S., 2020. Developments toward the implementation of ^{44}Sc production at a medical cyclotron. Molecules 25, 1–16. http://dx.doi.org/10.3390/molecules25204706.

Mirion Technologies, 2022. GENIE 2000 - Basic spectroscopy software. URL https://www.mirion.com/products/genie-2000-basic-spectroscopy-software. (Last access 12 October 2022).

Nesteruk, K.P., Auger, M., Braccini, S., Carzaniga, T.S., Ereditato, A., Scampoli, P., 2018. A system for online beam emittance measurements and proton beam characterization. J. Instrum. 13, P01011. http://dx.doi.org/10.1088/1748-0221/13/01/p01011.

Potkins, D.E., Braccini, S., Nesteruk, K.P., Carzaniga, T.S., Vedda, A., Chiodini, N., Timmermans, J., Melanson, S., Dehnel, M.P., 2017. A low-cost beam profiler based on cerium-doped Silica fibers. Physics Procedia 90, 215–222. http://dx.doi.org/10.1016/j.phpro.2017.09.061.

Renaldin, E., Dellepiane, G., Braccini, S., Sommerhalder, A., Hui, Z., van der Meulen, N.P., Eichler, R., Talip, Z., 2023. Cyclotron production of medically relevant radionuclide thulium-167. Front. Chem. (in preparation).

Sadeghi, M., Enferadi, M., Tenreiro, C., 2010. Nuclear model calculations on the production of Auger emitter ^{165}Er for targeted radionuclide therapy. J. Mod. Phys. 1 (4), 217–225. http://dx.doi.org/10.4236/jmp.2010.14033.

Sadler, A.W.E., Hogan, L., Fraser, B., Rendina, L.M., 2022. Cutting edge rare earth radiometals: prospects for cancer theranostics. EJNMMI Radiopharm. Chem. 7 (1), 21. http://dx.doi.org/10.1186/s41181-022-00173-0.

Sandia National Laboratories, 2022. InterSpec - spectral radiation analysis software. URL https://sandialabs.github.io/InterSpec/. (Last access 12 October 2022).

Tárkányi, F., Hermanne, A., Király, B., Takács, S., Ditrói, F., Baba, M., Ohtsuki, T., Kovalev, S., Ignatyuk, A., 2007. Study of activation cross-sections of deuteron induced reactions on erbium: Production of radioisotopes for practical applications. Nucl. Instrum. Methods Phys. Res. B 259 (2), 829–835. http://dx.doi.org/10.1016/j.nimb.2007.01.287.

Tárkányi, F., Hermanne, A., Takács, S., Ditrói, F., Király, B., Kovalev, S., Ignatyuk, A., 2008a. Experimental study of the ^{165}Ho(d,2n) and ^{165}Ho(d,p) nuclear reactions up to 20 MeV for production of the therapeutic radioisotopes ^{165}Er and ^{166g}Ho. Nucl. Instrum. Methods Phys. Res. B 266 (16), 3529–3534. http://dx.doi.org/10.1016/j.nimb.2008.05.123.

Tárkányi, F., Hermanne, A., Takács, S., Ditrói, F., Király, B., Kovalev, S., Ignatyuk, A., 2008b. Experimental study of the ^{165}Ho(p,n) nuclear reaction for production of the therapeutic radioisotope ^{165}Er. Nucl. Instrum. Methods Phys. Res. B 266 (15), 3346–3352. http://dx.doi.org/10.1016/j.nimb.2008.05.005.

Tárkányi, F., Hermanne, A., Takács, S., Király, B., Spahn, I., Ignatyuk, A., 2010. Experimental study of the excitation functions of proton induced nuclear reactions on ^{167}Er for production of medically relevant ^{167}Tm. Appl. Radiat. Isot. (ISSN: 0969-8043) 68 (2), 250–255. http://dx.doi.org/10.1016/j.apradiso.2009.10.043.

Tárkányi, F., Takács, S., Hermanne, A., Ditrói, F., Király, B., Baba, M., Ohtsuki, T., Kovalev, S., Ignatyuk, A., 2008c. Study of activation cross sections of proton induced reactions on erbium for practical applications. Nucl. Instrum. Methods Phys. Res. B 266 (22), 4872–4876. http://dx.doi.org/10.1016/j.nimb.2008.08.005.

Tárkányi, F., Takács, S., Hermanne, A., Ditrói, F., Király, B., Baba, M., Ohtsuki, T., Kovalev, S., Ignatyuk, A., 2009. Investigation of production of the therapeutic radioisotope ^{165}Er by proton induced reactions on erbium in comparison with other production routes. Appl. Radiat. Isot. 67 (2), 243–247. http://dx.doi.org/10.1016/j.apradiso.2008.10.006.

Yasui, L., Hughes, A., DeSombre, E., 2001. Relative biological effectiveness of accumulated ^{125}IdU and ^{125}I-estrogen decays in estrogen receptor-expressing MCF-7 human breast cancer cells. Radiat. Res. 155 (2), 328–334. http://dx.doi.org/10.1667/0033-7587.

Zandi, N., Sadeghi, M., Afarideh, H., 2013. Evaluation of the cyclotron production of ^{165}Er by different reactions. J. Radioanal. Nucl. Chem. 295, 923–928. http://dx.doi.org/10.1007/s10967-012-2116-0.

Ziegler, J., Manoyan, J., 1988. The stopping of ions in compounds. Nucl. Instrum. Methods B35, 215. http://dx.doi.org/10.1016/0168-583X(88)90273-X.